Combined photocatalytic degradation of pollutants and inactivation of waterborne pathogens using solar light active /-Bi2O3

Combined photocatalytic degradation of pollutants and inactivation of waterborne pathogens using Solar Light Active α/β-Bi_2O_3

Najeebullah Channa[a], Tanveer A. Gadhi[a*], Rasool Bux Mahar[a], Alessandro Chiadò[b*], Barbara Bonelli[b], Alberto Tagliaferro[b,c]

[a]U.S. Pakistan Center for Advanced Studies in Water (USPCASW), Mehran, University of Engineering and Technology, Jamshoro 76062, Pakistan.

[b]Department of Applied Science and Technology, Politecnico di Torino, Corso Duca degli Abruzzi 24, 10129 Torino, Italy.

[c]Faculty of Science, Ontario Tech University, 2000 North Simcoe Street, Oshawa, Ontario L1G 0C5, Canada.

[*]Corresponding Authors Email: alessandro.chiado@polito.it and tanveer.uspcasw@admin.muet.edu.pk

Abstract

A solar light active composite of α/β-Bi_2O_3 was synthesized using a chemical-free solid-state reduction method. The obtained composite was characterized by X-ray diffraction, UV-Vis spectroscopy, field emission scanning electron microscopy, and zeta potential. Initially, to validate the photocatalytic effectiveness, the obtained α/β-Bi_2O_3 composite was used to degrade indigo carmine dye. Then, the inactivation of *E. coli* and *S. aureus* waterborne pathogens was performed on solid and in liquid media. On solid agar media, a significant inhibition zone was observed for both bacterial strains. Similarly, in liquid culture, these strains *E. coli* and *S. aureus* were reduced from 1×10^6 CFU/mL to a few CFU/mL, after 240 min of photocatalytic exposure. Furthermore, mixed wastewater of indigo carmine and *E. coli*/*S. aureus* were tested to study the combined photocatalytic mechanism against the organic dye and microorganisms. Overall, the obtained results suggested the efficacy of α/β-Bi_2O_3 towards visible light inactivation of bacteria even in combination with other pollutants, highlighting the great potential of the advanced photocatalytic process for combined treatment of organic pollutants and pathogens.

Keywords: Antibacterial, waterborne pathogens, α/β-Bi_2O_3, Photocatalysis, Wastewater.

1. Introduction

The anthropogenic and industrial activities produce in their wastewater (WW) high loads of organic and inorganic compounds, such as dyes, resins, metals, nutrients and pathogenic bacteria, as well as other by-products, classified as new emerging contaminants, like drugs and antibiotics [1, 2]. The presence of these pollutants resulted in cross-contamination to surface water bodies with organic and inorganic compounds alongside pathogens. For such a mixed stream, pathogens' removal needs immediate attention due to the risk of waterborne diseases and the possibility of microorganisms to develop antibiotic resistance [3, 4]. Many treatment systems and techniques are available to remove pathogens from drinking water or WW, such as chlorination and ultraviolet (UV) light [5, 6]. Chlorination is mostly applicable to all water systems, but it produces toxic by-products, and some of them are carcinogens [7]. UV disinfection methods are widely used because of their efficacy with a targeted attack on the DNA or RNA of the bacterial cells. However, the UV treatment has some limitations, such as the high costs, the energy requirements, and the reduced interactive exposure for bulk applications [8, 9].

Heterogeneous photocatalysis is an advanced oxidation process considered a green approach. Indeed, it applies the irradiation and activation of photocatalytic materials via UV/solar light to generate reactive oxygen species (ROS) for the degradation and treatment of contaminants, and some studies reported as well a bacterial inactivation using photocatalytic metal oxide nanoparticles (e.g. titanium, copper, and zinc-based) [10-12]. In principle, ROS attacks the cell wall/membrane and results in bacterial cells' damage as revealed for instance by live/dead cell viability using fluorescence microscopy [10, 11]. In a nutshell, all of these works highlight that there is a constant need for efficient and stable photocatalytic active materials that could reduce the water pollution problem and all of its consequences, including various diseases resulting from pathogenic bacteria [11]. However, most of the mentioned studies focused on either antimicrobial activity or the removal and degradation of organic/inorganic pollutants alone. Considering the mixed nature of WW, rare work has been done on evaluating simultaneously the photocatalytic antibacterial activity and organic pollutant degradation i.e. when the bacteria and organic compounds are found together and interfering with each other.

Bismuth-based materials are widely studied for the photocatalytic degradation of organic compounds [13-15]. Bismuth oxide (Bi_2O_3) has six polymorphic crystalline structures i.e. α, β, δ, γ, ε and ω: the α and β phases were mostly investigated for photocatalytic applications [15]. It has

been reported that Bi_2O_3 has better solar/visible light efficiency due to the wide absorption spectrum in the visible region and optimum optical energy bandgap, if compared to other metal oxides. For instance, compared to pristine TiO_2, the Bi_2O_3 photocatalytic activity is two times higher under visible light [16].

In the present study, the use of solar light active α/β-Bi_2O_3 composite, earlier reported for degradation of organic compounds [17], was investigated for bacterial inactivation alone or combined with an organic dye, to simulate a real mixed WW. To the best of our knowledge this is one of the first attempt for the combined degradation of organic pollutants and pathogens. The α/β-Bi_2O_3 composite was synthesized by using a chemical-free solid-state thermal reduction method. The synthesized bulk composite was characterized by X-ray diffraction (XRD) for the analysis of crystal phase and composition, by UV-Vis spectroscopy for the optical properties, by scanning electron microscopy to assess the morphological structure and zeta potential for the surface charge properties. The obtained composite was initially tested for the photocatalytic degradation of indigo carmine (IC) dye under visible light and afterward evaluated for the antibacterial potential against two bacterial strains i.e. the Gram-positive *S. aureus* and the Gram-negative *E. coli,* by using the plate count method and fluorescence microscopy.

2. Material and methods

2.1 Materials

Precursor salt of bismuth ($Bi(NO_3)_3{:}5H_2O$), triethylamine (TEA), p-benzoquinone (BQ), isopropanol (IP) and Indigo Carmine (IC) were purchased from Sigma-Aldrich, Italy, and used as received. Ethanol and sodium chloride (NaCl, 99.5%) were purchased from Daejung, China. For the bacterial analysis, Luria-Bertani (LB) agar and broth and Tryptone Soya broth (TSB) were purchased from Oxoid, England. The LIVE/DEAD® BacLight™ Bacterial Viability Kit was purchased from Thermo Fisher Scientific, USA, for the live/dead cell staining.

2.2 α/β-Bi_2O_3 synthesis

The α/β-Bi_2O_3 composite was synthesized in bulk powder form, using a previously reported method that employed thermal decomposition of $Bi(NO_3)_3{\cdot}5H_2O$ [17]. In brief, a measured quantity of $Bi(NO_3)_3{\cdot}5H_2O$ salt was directly heated at 150 °C for 30 min in the muffle furnace i.e. to evaporate the moisture content. Afterward, the temperature was increased to 250 °C and kept

for 2 hours. Finally, the resultant salt was calcined at 550 °C for 2 hours and allowed for ambient cooling inside the furnace to obtain the thermally reduced and calcined bulk α/β-Bi_2O_3 composite.

2.3 Characterization

The as-calcined powder morphology was investigated through a MERLIN ZEISS field-emission scanning electron microscopy (FESEM). The calcined powders were analyzed using X-ray diffraction (XRD) to investigate both the crystalline structure and phase's composition. The UV-Vis diffuse reflectance spectra were recorded by using a Varian Cary 5000 spectrophotometer (Agilent Technologies). The Tauc plots of the Kubelka Munk function were used to calculate the energy band gap (E_g) value. The Brunauer−Emmett−Teller (BET) specific surface area of the obtained powder was measured through N_2 adsorption at 77 K on a Micromeritics Tristar-II instrument. The zeta potential was measured through Malvern-Zetasizer, at neutral pH.

2.4 Photocatalytic removal of indigo carmine

To confirm the synthesized α/β-Bi_2O_3 photocatalytic activity, initially, the degradation of the IC dye was evaluated under a white LED lamp (Phillips, emission spectrum ranging from 430 to 800 nm) with an irradiance of 100 W/m^2, placed 45 cm far from the dye solution. The IC dye concentration was kept at 10 ppm, within a solution of 50 mL; the α/β-Bi_2O_3 loading in the dye solution was 1 mg/mL (1:1). In the beginning, the suspension was stirred for 30 min in the dark for adsorption-desorption equilibrium before exposure to irradiation. The dye solution's absorbance spectra were recorded with different irradiation time intervals using a UV-Vis spectrophotometer (Shimadzu 1800) by taking an aliquot of 3 mL centrifuged at 10,000 rpm for 3 min. The powder sample and aliquot were returned to the vial to preserve the same powder and solution amount. The amount of IC dye removed during the treatment was estimated from the decrease of the absorbance at 610 nm, corresponding to the principle peak in the spectra of the dye. In order to confirm the dependence of ROS on the photocatalytic degradation of the dye, such tests have been repeated in the presence of known ROS scavengers/quencers (4% w/v) in the IC dye solution: TEA for quenching h^+, BQ for the reactive oxygen ($O_2^{\bullet-}$) and IP for the OH^- radicals.

2.5 Preparation of Bacterial Culture

Two bacterial strains were used to analyze the antibacterial activity by α/β-Bi_2O_3: *E. coli* (ATCC 8739), a Gram-negative considered an indicator of contaminations by bacteria in fresh/seawater

and *S. aureus* (ATCC 25923), a Gram-positive pathogenic bacterial strain generally found not only in WW but even in hospital infections. *E. coli* was cultured in LB broth (Oxoid) [18], whereas *S. aureus* was inoculated into TSB (Oxoid) [19, 20]. Afterward, both bacterial strains were grown overnight in a shaker at 37 °C and 120 rpm.The day after, 50 mL of both strains' broth culture were placed in the centrifuge tubes and centrifuged at 5000 rpm for 15 minutes. Bacterial biomass was separated and washed several times with sterile 0.85% NaCl solution [21], then diluted in the same saline solution to get a final bacterial suspension of 50 mL prepared at the concentration of 1×10^6 colony forming unit per mL (CFU/mL).

2.6 Photocatalytic bacterial inactivation

2.6.1 Antibacterial tests on solid media

The antibacterial tests of *E. coli* and *S. aureus* were conducted using a modified Kirby–Bauer test, by placing the powders directly on agar without any filter disk in between. The bacterial inoculum (100 µL) at the concentration of 1×10^6 CFU/mL was spread on LB agar plates for both strains. The test was then performed in the dark or under the same white LED lamp used for dye degradation (see 2.4). In brief, 10 mg of α/β-Bi_2O_3 powder was placed in defined circular spots on the bacteria inoculated petri dishes and then incubated overnight at 37 °C under dark conditions or irradiated with the LED lamp. The zone of inhibition was calculated based on the method reported in [22].

2.6.2 Antibacterial tests in liquid media

For photocatalytic evaluation of the inactivation of the same bacterial strains in liquid cultures, 50 mg of α/β-Bi_2O_3 powder was added to 50 mL of the above-mentioned bacterial suspension at a concentration of about 1×10^6 CFU/mL. The resulted suspension (of α/β-Bi_2O_3 powder and bacteria) was stirred in the dark for 30 minutes. Afterward, the photocatalytic response was observed with and without the presence of α/β-Bi_2O_3 under the LED lamp at about 25 °C, following the same conditions used for dye degradation (see 2.4). A “dark control” (the bacterial suspension incubated with the nanomaterial in the dark), was also included. 100 µL of microbial suspensions were drawn from each tested condition after 30, 60, 120, 240 min, and were serially diluted. Finally, 100 µL of each serially diluted samples were spread on the respective agar plates and incubated overnight at 37 °C for analyzing the reduction in bacterial growth respective to different

treatment time. Moreover, to analyze the stability and reuse potential of the recovered bismuth-based nanomaterial, the tested α/β-Bi_2O_3 powder was recovered, washed, dried, and reused up to 3-cycles for antibaterial tests on solid media (as reported above).

2.6.3 Photocatalytic degradation of mixed pollutants and pathogens in an artificial WW

For the photocatalytic evaluation of an artificial WW i.e. containing IC dye and *E. coli or S. aureus*, the stock solution was prepared by adding 5 ppm of IC in sterilized 0.85% NaCl. The overnight grown culture of *E. coli* and *S. aureus* was centrifuged to separate the pellets from the broth. Then, the separated pellets were washed with 0.85 % NaCl solution and resuspended in 50 mL of the prepared stock solution of IC to make two mixed WW solutions i.e. one of IC and *E. coli*, and another of IC and *S. aureus*. The initial concentration of bacteria in the mixed WW was maintained at around 1×10^6 CFU/mL. For photocatalytic evaluation, the α/β-Bi_2O_3 powder was added in the mixed WW, and the obtained slurry was initially stirred in the dark for 30 min. Afterward, the irradiation was started, and the samples were collected after different exposure time, centrifuged, and analyzed for removal of IC. The collected samples were serially diluted for bacterial reduction analysis through the plate count method and live/dead cell staining using fluorescence microscopy (see 2.7). All the experiments and analyses were performed at least twice for the reproducibility of obtained results.

2.7 Fluorescence microscopy

During photocatalytic exposure, along with the bacterial density reduction analysis, the withdrawn samples were analyzed for live/dead bacterial cell staining by using the LIVE/DEAD® BacLightTM Bacterial Viability Kit and fluorescence microscopy. This kit includes the SYTO 9, a dye that stains green on a fluorescence microscope in a live bacterial cell, and another dye, propidium iodide (PI) stains red in case of a dead bacterial cell. The method for fluorescence analyses was followed as per the guidelines provided by the viability kit supplier. In brief, 1 mL of the treated suspension (i.e. a mixture of bacterias and α/β-Bi_2O_3) was drawn after 0, 30, 60, 120, and 240 min, and centrifuged at 10,000 × g for 10 minutes, then the supernatant was drained. Further, the obtained bacterial biomass was washed with a sterile washing buffer solution, centrifuged again, and resuspended and vortexed with 1 mL of 0.85% NaCl. Then, 3 µL of the mixed dye solution (PI: SYTO 9-1:1 (v:v)), was added to the resuspended solution, vortexed for thorough mixing, and incubated for 15 minutes in dark conditions and at room temperature.

Afterward, 5 µL of the stained suspension was pipetted onto a sterilized glass slide and analyzed on a Zeiss fluorescence microscope (Zeiss Axio Scope. A1 Carl Zeiss Germany). The FITC and Texas Red filters were used for acquiring the stained live and dead cells images, respectively. The acquired images of live and dead cells were analyzed using ImageJ 1.50d to assess the percentage of live (green stained) and death (red stained) bacterial cells.

3. Results and Discussion

3.1 Characterization of synthesized α/β-Bi_2O_3

At first, the obtained powder was characterized using XRD, UV-Vis spectroscopy, FESEM, and zeta potential to investigate the composition of the crystal phase and the optical, morphological, and surface charge properties. Afterward, it was tested for photocatalytic removal of IC dye and bacteria.

3.1.1 XRD

The XRD pattern of the as-synthesized powder sample at 550 °C and commercial α-Bi_2O_3 and β-Bi_2O_3 powders are shown in Fig. 1A. Most of the peaks correspond to monoclinic-α-Bi_2O_3, with principal peaks at 27.06, 27.52, 33.9° (JCPDS card no. 01-071-0465). Additionally, some peaks due to tetragonal β-Bi_2O_3 at 27.96, 41.36, 46.22 and 55.45° (JCPDS card no. 01-078-1793) were also found, showing the occurrence of a mixed composition of two different phases i.e. α and β with the formation of an α/β-Bi_2O_3 composite material of i.e. with around 20% proportion of β-phase [17]. Most of the XRD peaks with minor intensity are ascribed to α-Bi_2O_3 as revealed after detailed analysis through the PDXL2 software and comparison to XRD patterns of the commercial α-Bi_2O_3 powders.

It is known that when the metastable β-Bi_2O_3 phase is cooled down from high temperatures to ambient conditions, it is usually transformed into α- Bi_2O_3 unless some dopants, such as Tantalum or Niobium, are introduced to stabilize the metastable β-phase at room temperature [23-25]. In one of our studies [26], we established that the Nitrogen present in the precursor salt has a β-Bi_2O_3 stabilizing role. Indeed, the formation of α/β-Bi_2O_3 can be associated with the decomposition of the the precrursor salt ($Bi(NO_3)_3{\cdot}5H_2O$) at increased temperature, with a consequential loss of NO and O_2. With the complete decomposition of NO above 540 °C [26], some traces of N could remain in the bulk synthesized Bi_2O_3, stabilizing some of the β-Bi_2O_3 at room temperature (i.e. after most

of the transformation in α-Bi_2O_3) and resulting in the formation of a composite heterostructure of α/β-Bi_2O_3 [17].

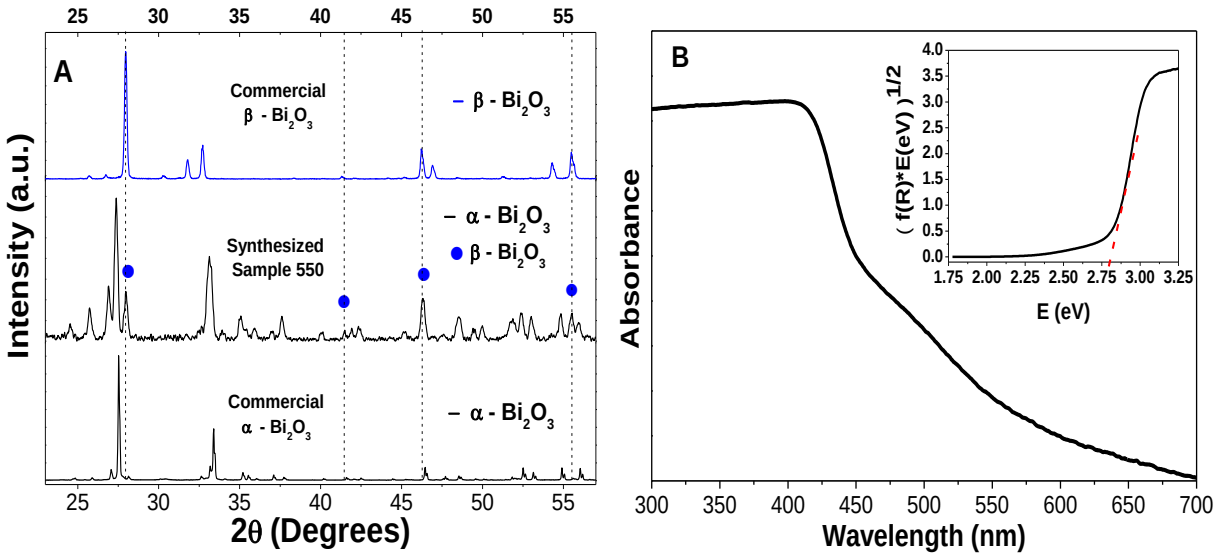

Fig. 1 A) XRD pattern of synthesized bulk α/β-Bi_2O_3, compared to commercial powders. B) UV-Vis DRS analysis of the synthesized α/β-Bi_2O_3, and the inset shows the Tauc plot obtained from Kubelka-Munk method.

3.1.2 Optical properties

Fig. 1B shows the diffused reflectance UV-Vis spectroscopy (DRS) analysis of the synthesized sample, and the inset shows the corresponding Tauc plot. The broad spectrum in the region from 400 to 450 nm is attributed to α-Bi_2O_3, while the additional plateau i.e. from 470 to 550 nm displayed the contribution of β-Bi_2O_3 [17]. In principle, these absorptions are associated with the composite electronic transition from the valence band to the conduction band [17]. The estimated bandgap energy of α/β-Bi_2O_3 was around 2.78 eV (shown in the inset Fig. 1B); the presence of the heterojunction of β-phase influenced the slight reduction in the bandgap. Overall, considering the band gap value and the corresponding optical transition in the visible region, these data confirm that the nanomaterial can be fruitfully activated by visible light.

3.1.3 Morphology

Fig. 2 shows the FESEM images of α/β-Bi_2O_3 at different magnification scales, presenting the typical morphology of Bi_2O_3 materials with layered interconnected and flowery microstructure. A similar morphology of bismuth oxides is also reported in various studies [27, 28]. The observed thickness of the interconnected layers was around 30-45 nm. Interestingly, the tiny voids and

spaces between the interconnected layers revealed some macroporosity of the composite material, facilitating interaction with contaminants for improved photocatalytic performance.

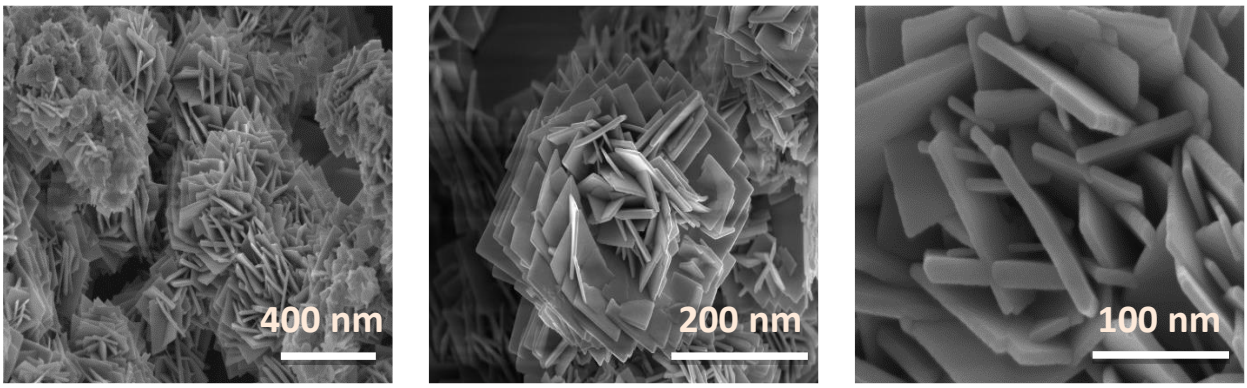

Fig. 2 FESEM images of α/β-Bi_2O_3 at different magnification scales

3.1.4 Surface characteristics

At neutral pH, the observed zeta potential of the α/β-Bi_2O_3 composite was around -35 mV, suggesting that the negative net charge of the scattering sites around the composite surface could facilitate the interaction with positively charged ions/molecules and, at the same time, could attain better colloidal stability in a suspension [29]. In addition, the zeta potential was analyzed at different pH; the obtained values were plotted and given in Fig. S1. In strong acidic conditions i.e. at pH=2, the net negative charge of the α/β-Bi_2O_3 was stabilized to zero due to abundant availability of H^+ ions. On the contrary, at basic pH (=10), the negative ionic surface characteristic was increased due to the abundance of OH^- ions on the α/β-Bi_2O_3 surface, reaching a value of about -47 mV.

Moreover, the recorded BET specific surface area of the α/β-Bi_2O_3 composite was in the range of 7.6 m^2/g, which suggests that the obtained composite is not porous and will allow minimum adsorption on the surface or within the macropores (shown in FESEM images, Fig. 2).

3.2. Photocatalytic removal of Indigo Carmine (IC)

Fig. 3A shows the absorbance spectrum of the IC dye at different irradiation times in the presence of the α/β-Bi_2O_3 composite under visible light, while Fig. 3B shows the relative concentration and kinetic profile of IC dye. The obtained kinetics revealed that IC's removal follows a 1^{st} order linear degradation kinetics and a calculated kinetic apparent rate (K_{app}) of 3.67 x 10^{-2} min^{-1}. In our earlier

work [17, 30], the IC dye's degradation mechanism was explained in detail; in brief, the oxidation species attacked the IC dye and dissociated into amine-sulfo-benzoic acid and isatin sulfonic acid and partially mineralized to carboxylic groups and phenol derivatives [30-32].

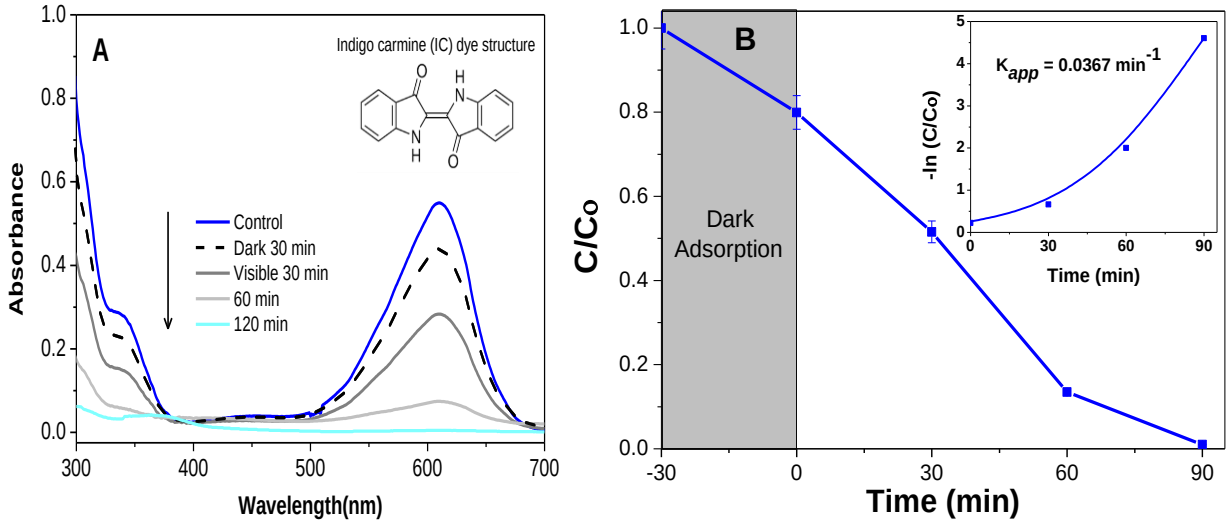

Fig. 3 A) Absorbance spectra of the IC dye removal using α/β-Bi_2O_3 under LED lamp; B) relative concentration decrease at different treatment time (considering the optical density at 610 nm; each point is the average of two replicates); inset: kinetic curve plot and calculated kinetic apparent constant (Kapp).

3.3 Photocatalytic bacterial inactivation on solid and liquid media

Once the composite was proved to be effective towards an organic dye, the main focus was to evaluate the photocatalytic inactivation of bacteria using the α/β-Bi_2O_3 composite. Therefore, two pathogen indicators (commonly found in drinking water) i.e. *E. coli* and *S. aureus* were selected. The observed inhibition halo for both bacterial strains is shown in Fig. 4A. Compared to the biotic control (without the presence of α/β-Bi_2O_3), the petri dishes with the presence α/β-Bi_2O_3 showed growth inhibition of both *E. coli* and *S. aureus* under the LED light irradiation, showing an inhibition halo for *E. coli* and *S. aureus* of around 11 mm and 10 mm, respectively. These results revealed the potential of α/β-Bi_2O_3 towards inhibition of both bacterial strains.

Due to the well-known limitations (e.g. mass transfer limitations, absorption, and complexation to organic compounds) that affect metal bioavailability during tests on solid media [33], the effectiveness of the α/β-Bi_2O_3 composite was evaluated in liquid cultures, too. The obtained results, obtained by assessing the number of CFU/mL (shown in Fig. 4B), confirmed the bacterial cell density reduction for both strains after 240 min of photocatalytic exposure. Indeed, the initial

bacterial density (1×10^6 CFU/mL for both strains) was significantly reduced (about 99.99% reduction) for both *E. coli* and *S. aureus*, respectively. However, the reduction was found higher in the case of *E. coli*. A "dark control" in which the bacterial suspension was mixed with the nanomaterial but incubated in the dark, was also included for each strain. The cell densities recorded during time for these dark controls were comparable to those obtained by the controls cultured under the visible light, but in the absence of the α/β-Bi_2O_3 composite.

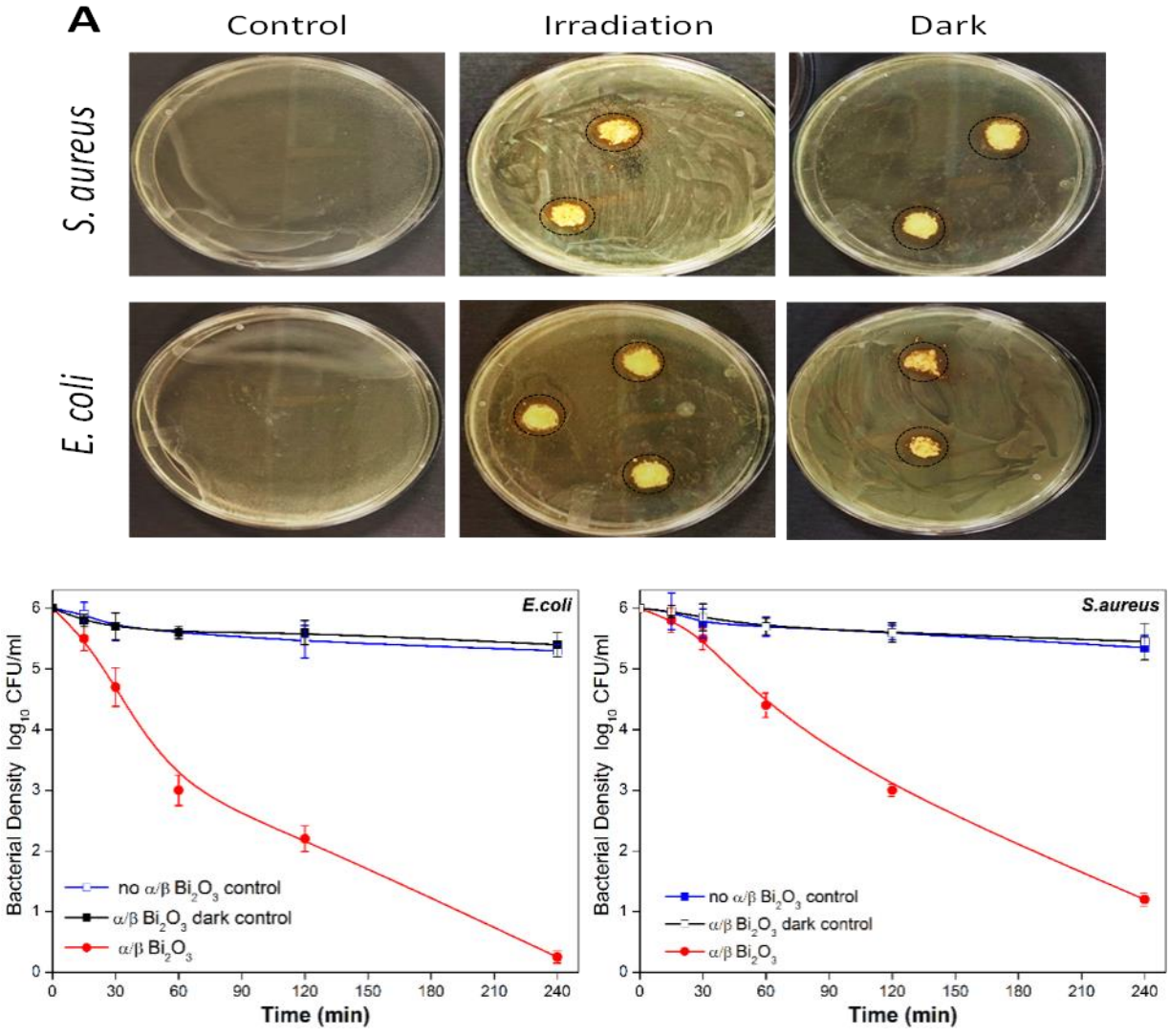

Fig. 4 A) Photocatalytic inhibition of *E. coli* and *S. aureus* on solid media in the presence of α/β-Bi_2O_3 under visible light irradiation; B) Bacterial density (CFU/mL) reduction of *E. coli* (EC, left) and *S. aureus* (SA, right) liquid suspensions incubated under visible light with and without (control) the presence of α/β-Bi_2O_3. A "dark control" (bacterial suspension incubated with the nanomaterial in the dark), was also included.

3.4 Fluorescence microscopy of live/dead bacterial cells

To confirm if the α/β-Bi_2O_3 has a biocidal effect on the bacterial strains, live/dead staining was adopted in combination with fluorescence microscopy. The fluorescent green-stained cells represent live cells, whereas the red-stained represent dead ones. The acquired merged live/dead fluorescence microscopy images of *E. coli* (top), and *S. aureus* (bottom) are shown in Fig. 5, while the separate live and dead stained cells are shown in supplementary data Fig. S2. For both strains, in the beginning, plenty of live green-stained cells could be observed, even if the number of dead cells (red-stained) start to increase already after 15 minutes for both strains. In contrast, at increasing photocatalytic exposure, the bacterial cells in the presence of α/β-Bi_2O_3 resulted in the cell membrane's rupture, as indicated by the increasing number of red stained cells during the treatment. The increased appearance of red-stained cells at longer exposures revealed that α/β-Bi_2O_3, along with growth inhibition, could kill both bacterial strains. Potentially, during the photocatalytic reaction, the nanomaterial produces ROS that could attack the bacterial cell and leads to bacterial cell damage that increased the permeability of the membrane to PI staining [11].

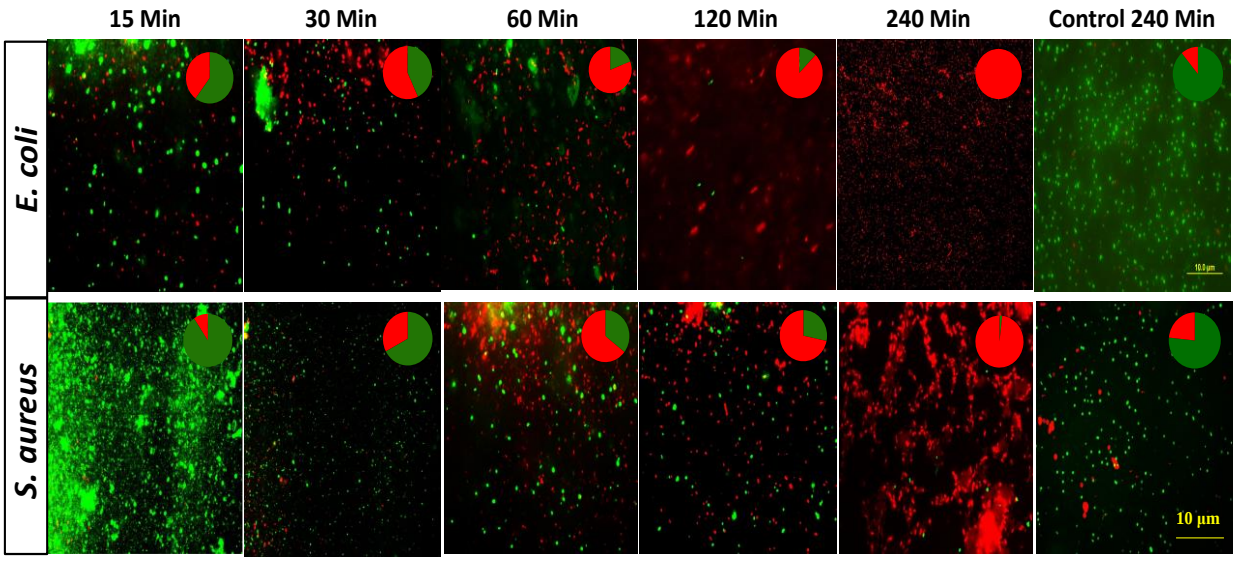

Fig. 5 Merged live/dead fluorescence microscopy images of *E. coli* and *S. aureus* at different treatment times: 15 min, 30 min, 60 min, 120 min, 240 min, and images of controls (without α/β-Bi_2O_3) after 240 min.

Compared to the obtained results in Fig. 4B, the fluorescence images in Fig. 5 confirmed a similar trend of higher inactivation of *E. coli* cells than the *S. aureus*. For instance, by comparing the values obtained after 60 minutes of treatments, the higher inactivation of *E. coli* result significant

if compared to that of *S. aureus* (p value= 0.0467). The estimated proportions of live and dead cells of both strains i.e. after prolonged photocatalytic exposure of 240 min, are given in Table 1, which again revealed an increased proportion of dead cells over live in the case of *E. coli*. Anyway, for both strains, the time required for the complete sanitation of water can be compatible with standard WW treatments.

Table 1. Proportions of live and dead bacterial cells at different treatment times.

Time (min)	*E. coli*		*S. aureus*	
	Live %	Dead %	Live %	Dead %
15	60.24 ± 4.07	39.76 ± 1.23	90.56 ± 12.89	9.44 ± 1.74
30	43.04 ± 3.32	56.96 ± 1.40	67.19 ± 9.21	32.81 ± 5.27
60	19.12 ± 1.94	80.88 ± 1.69	35.47 ± 1.28	64.53 ± 4.19
120	12.33 ± 0.18	87.67 ± 5.19	28.31 ± 1.05	71.69 ± 3.19
240	0.33 ± 0.06	99.67 ± 14.47	1.90 ± 0.02	98.10 ± 2.42
Control*	88.96 ± 0.76	11.04 ± 0.25	77.12 ± 2.35	22.88 ± 0.63

* The control corresponds to a bacterial suspension irradiated with visible light for 240 minutes, without the photocatalyst's presence.

3.5 Photocatalytic degradation of mixed pollutants and pathogens in an artificial WW

To investigate the photocatalytic response towards IC and bacteria's combined presence, mixed WW of IC and *E. coli*/*S. aureus* were tested with and without the presence of α/β-Bi_2O_3. The obtained results of this artificial WW for both bacterial strains are shown in Fig. 6. As compared to the previous results of IC removal alone, the removal kinetics of IC was reduced in the mixed WW i.e. from 3.67 x 10^{-2} min^{-1} to 0.8 x 10^{-2} min^{-1}, as estimated from the relative concentration decrease in Fig. 6A. The decreased kinetics was probably due to the relative optical density of bacterial suspension that hindered the irradiation passage and α/β-Bi_2O_3 activation, and besides, limited reactive species that could have simultaneously targeted both the bacteria and IC dye molecule and reduced the overall kinetics. Further, Fig. 6B shows the control of both mixed WW solutions i.e. with and without the presence of α/β-Bi_2O_3, the bacterial growth of both bacteria remained unaffected due to the presence of IC. Compared to the previous results (Fig. 4B), almost a similar bacterial density reduction trend was observed for both bacterial strains. The inactivation

was more effective towards *E. coli* than *S. aureus*. The control of all the mixed WW showed little change in either removing IC (alone and in the mixed WW) or in the bacterial density after prolonged exposure of irradiation under LED lights if the composite was not added. The overall results revealed that the presence of bacteria interfered with the photocatalytic degradation and removal of the organic compound, as observed by reduced IC dye kinetics in the mixed WWs. On the contrary, the inactivation of both bacterial strains was unaffected in the presence of IC, as the observed density reduction trend was similar compared to the bacterial suspension without the presence of IC dye.

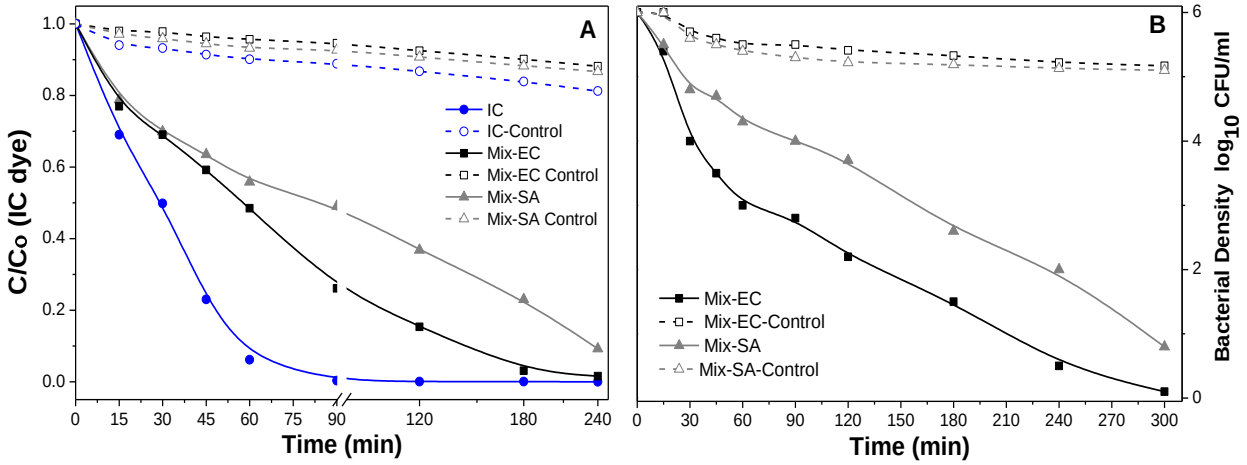

Fig. 6. A) Relative concentration decrease of IC alone and in mixed wastewater (WW) with *E. coli*/*S. aureus* with and without the presence of α/β-Bi_2O_3; B) Bacterial density reduction of both *E. coli* and *S. aureus* in mixed WW with IC with and without the presence of α/β-Bi_2O_3 (Mix-EC referred to a mixed WW of IC and *E. coli*, Mix-SA is referred to a mixed WW of IC and *S. aureus*.

3.6 Stability and reuse of α/β-Bi_2O_3

To evaluate the α/β-Bi_2O_3 powder's reuse and stability potential, it was recovered, washed, dried, and reused for up to 3-cycles, for antibaterial tests on solid media and to observe any change in photocatalytic response. The observed inhibition zone on inoculated petri dishes in the presence of the recovered α/β-Bi_2O_3 powder, shown in supplementary data Fig. S3, revealed the stability and reusability of α/β-Bi_2O_3 for subsequent cycles of photocatalytic inactivation. This result highlight that this nanomaterial can be used more than one time, which is an advantage in the case of WW plants.

3.7 Photocatalytic mechanism

From the overall results, the encountered photocatalytic mechanism of action of the α/β-Bi_2O_3 powder can be explained. Previously, we reported that ROS were generated on the α/β-Bi_2O_3 surface due to resultant reactions of the photogenerated electrons (e^-) and holes (h^+) with the dissolved $O_2^{\bullet-}$ and $^{\bullet}OH$ radicals [17]. The cascade of photogenerated e^- and holes h^+ shown in Fig. 7 i.e., photocatalytic induced reactions, was facilitated due to heterojunction between α and β phases [17].

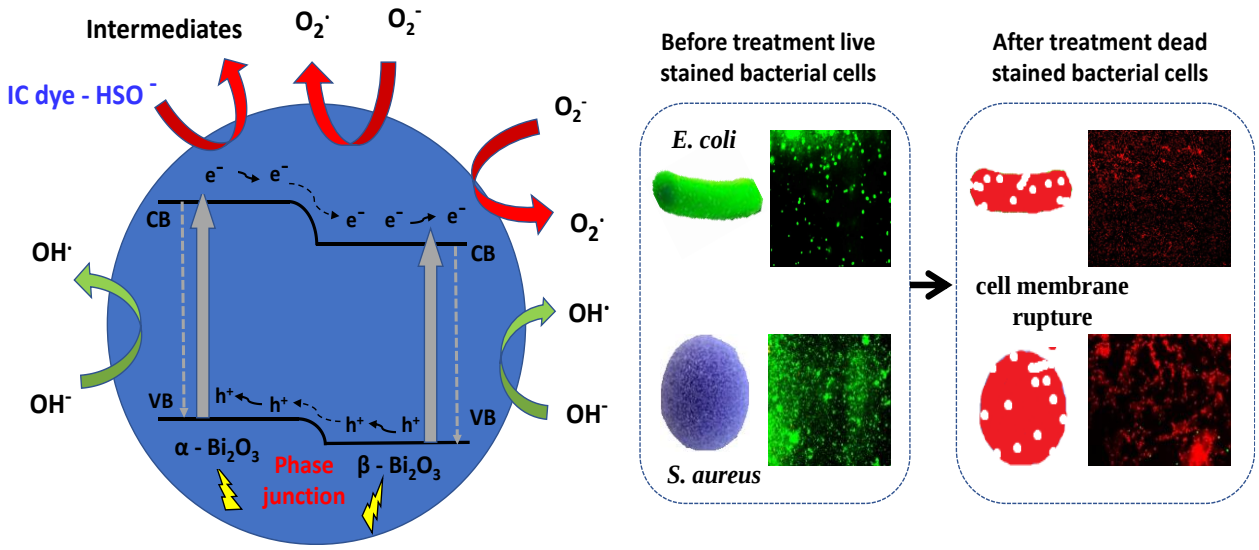

Fig. 7. Mechanism of origination of reactive species at α/β-Bi_2O_3 surface, degradation of IC dye, and inactivation of *E. coli* and *S. aureus* bacterial cells.

To further explore the photocatalytic activity and proof the oxidative/reductive paths, we did some photocatalytic tests with and without the addition of some reagents for the scavenging/quenching of holes and ROS. Indeed, some researchers have used TEA for quenching h^+, BQ for the reactive oxygen ($O_2^{\bullet-}$) and IP for the OH^- radicals [27, 34, 35], to observe any significant change in the degradation kinetics due to their presence in the dye solution. The addition of quenchers could influence the photocatalysis process i.e. by reducing the dye degradation kinetic rate because of the quenching of the generated reactive species or holes around the photocatalyst surface. Therefore, the degradation of the IC dye solution (10 ppm) was investigated under visible light, using α/β-Bi_2O_3, with and without the presence of these quenchers i.e. TEA, BQ, and IP.

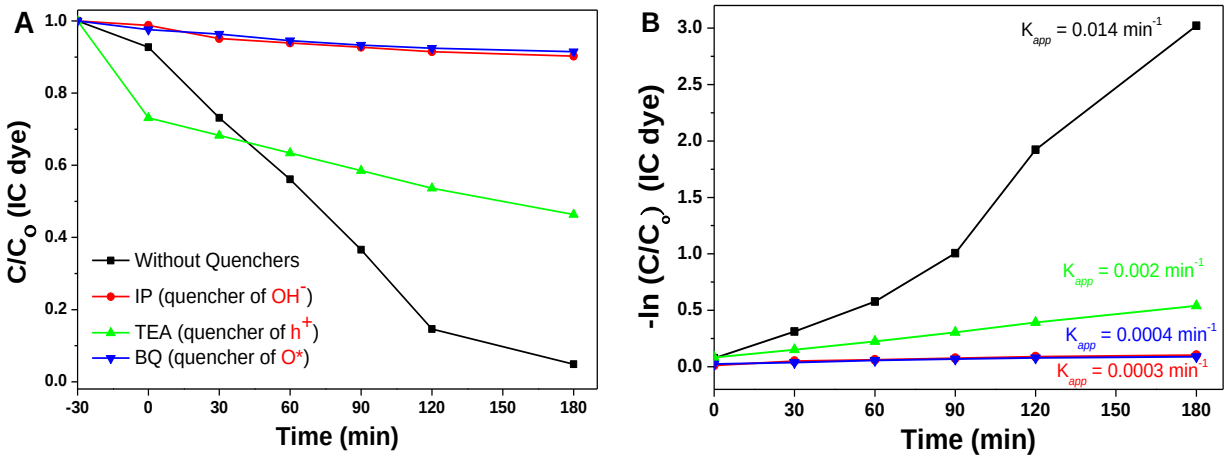

Fig. 8 A) Relative concentration of IC with and without quenchers; B) kinetic curves and K_{app}.

Fig. 8 show the C/C_o plots, and the kinetics curves along with the determined K_{app} of IC dye degradation with and without the quenchers in solution. It was observed that the degradation rate was drastically reduced in the presence of each quencher compared to the results without their addition, which revealed that both the $O_2^{\bullet-}$ and OH^- radicals were originated from the α/β-Bi_2O_3 surface and were responsible for the removal of the IC dye. Moreover, this also supports that the electrons are well separated from the h^+ in generating the reactive species quenched with quencher addition and decreasing degradation kinetics. The ROS originated on the α/β-Bi_2O_3 surface, probably could have degraded the organic dye, as well as the bacterial membrane/cell-wall [17, 36]. In the case of organic dyes, these reactions are responsible for partial or complete degradation of the parent molecule i.e. with the formation of intermediates and mineralization into CO_2, H_2O, NH_3 etc. [30, 36]. Instead, in the case of bacteria, the ROS, and in particular the hydroxyl radicals ($^{\bullet}OH$), the superoxide ($O_2^{\bullet-}$) and H_2O_2 originated by the photocatalytic reactions probably attacked the cell-wall/membrane and their constituents, resulting in different kinds of damage, as shown in the scheme given in Fig. 7. Indeed, it is widely known that these molecules can cause the peroxidation of lipids and phospholipids, as well as the oxidation of proteins present on the membranes [37]. These reactions can disrupt the membrane itself or simply its lipid bilayer organization, eventually leading to the efflux of cytosolic contents or cell lysis. Indeed, ROS have potent antimicrobial activity against bacteria, fungi and viruses, due to their quick action against various Gram-positive and Gram-negative bacteria, including multidrug-resistant strains [38]. This mechanism of action has been suggested for well-known metal such as silver [39], or other metal

oxides applied as antimicrobial [19]. Moreover, it is consistent with the earlier reported results of the efficacy of β-Bi_2O_3 on *E. coli* and *S. aureus* [21]. These strains belong to different microbial groups, namely Gram-negative and Gram-positive, and have different characteristics of cell wall/membrane thickness, morphology, and chemical groups [40]. Therefore, both bacteria's photocatalytic rupture could have occurred differently, as reported for TiO_2 [41]. The Gram-negative bacteria like *E. coli* has an outer membrane rich of lipopolysaccharides and phospholipids, a thin layer of peptidoglycan, and an inner phospholipidic membrane. Whereas, Gram-positive bacteria, like *S. aureus,* have a thick cell wall of peptidoglycans that covers the cytoplasmic membrane. Furthermore, it is well-known that bacteria belonging to *Staphylococci* groups can actively produce catalase, a heme protein enzyme that decomposes hydrogen peroxide to water and oxygen, protecting the cell from hydrogen peroxide-mediated leukocyte bactericidal mechanisms [42]. Moreover, *Staphylococci* can usually produce exopolysaccharides that could increase the resistance against the antibiotics and antimicrobial agents [43]. All of these considerations match with the obtained results. The high proportion of dead (red-stained) cells for both the treated strains suggested that the originated ROS could attack and inactivate both microorganisms through the cell wall/membrane's rupture. At the same time, *E. coli* was inactivated more rapidly than *S. aureus*, which appeared to be more resistant to the ROS originated by the α/β-Bi_2O_3 composite's photocatalytic action.

Conclusion

The α/β-Bi_2O_3 composite was obtained through facile solid-state thermal reduction of bismuth nitrate salt at 550 °C. The obtained composite with a balanced proportion of α-phase and the β-Bi_2O_3 phase contributed to the effective removal of IC dye and inactivation of Gram-negative *E. coli* Gram-positive *S. aureus*. In the presence of α/β-Bi_2O_3, the significant inhibition zone on the solid bacterial culture was observed, and bacterial cell density reduction in liquid suspension was achieved. The live/dead fluorescence microscopy analyses of the treated bacterial suspension revealed an almost complete biocidal effect after the prolonged photocatalytic exposure up to 240 min. Further, the photocatalytic evaluation of the mixed WW of IC and *E. coli*/*S. aureus* revealed that the removal kinetics of IC was affected and reduced due to interference of both bacteria, while the photocatalytic inactivation of both strains remained unaffected even with the presence of IC. Finally, even if a detailed photocatalytic investigation must be considered, the presented data

revealed that α/β-Bi_2O_3 was able to attack *E. coli* and *S. aureus* and showed the potential for the combined treatment of organic pollutants and microbial pathogens.

Acknowledgments

The authors acknowledge the technical support of Prof. Jennifer Weidhaas from the University of Utah, USA, Prof. Francesca Bosco, and Dr. Pravin Jagdale from Politecnico di Torino, Italy. This study was financially supported by the United States Government and the American people through the United States Agency for International Development (USAID) and USPCAS-W, MUET research project funding. The contents are the authors' sole responsibility and do not necessarily reflect the views of USAID or the United States Government.

References

1. Khatri, N. and S. Tyagi, *Influences of natural and anthropogenic factors on surface and groundwater quality in rural and urban areas.* Frontiers in Life Science, 2015. **8**(1): p. 23-39.
2. Hsiao, T.-C., et al., *Size distribution, biological characteristics and emerging contaminants of aerosols emitted from an urban wastewater treatment plant.* Journal of hazardous materials, 2020. **388**: p. 121809.
3. Chen, Z., et al., *Prevalence of antibiotic-resistant Escherichia coli in drinking water sources in Hangzhou city.* Frontiers in microbiology, 2017. **8**: p. 1133.
4. Kumar, M., et al., *Treatment enhances the prevalence of antibiotic-resistant bacteria and antibiotic resistance genes in the wastewater of Sri Lanka, and India.* Environmental research, 2020. **183**: p. 109179.
5. Hijnen, W., E. Beerendonk, and G.J. Medema, *Inactivation credit of UV radiation for viruses, bacteria and protozoan (oo) cysts in water: a review.* Water research, 2006. **40**(1): p. 3-22.
6. Di Cristo, C., et al., *Drinking water vulnerability assessment after disinfection through chlorine.* Procedia Engineering, 2015. **119**(1): p. 389-397.
7. Shin, D.-C., et al., *Assessment of Disinfection By-Products in Drinking Water in Korea.* Environmental health and toxicology, 2001. **16**(1): p. 1-8.
8. Kauser, I., M. Ciesielski, and R.S. Poretsky, *Ultraviolet disinfection impacts the microbial community composition and function of treated wastewater effluent and the receiving urban river.* PeerJ, 2019. **7**: p. e7455.
9. Mecha, A., et al., *UV and solar photocatalytic disinfection of municipal wastewater: inactivation, reactivation and regrowth of bacterial pathogens.* International journal of environmental science and technology, 2019. **16**(7): p. 3687-3696.
10. Raghunath, A. and E. Perumal, *Metal oxide nanoparticles as antimicrobial agents: a promise for the future.* International journal of antimicrobial agents, 2017. **49**(2): p. 137-152.
11. Das, S., et al., *Disinfection of multidrug resistant Escherichia coli by solar-photocatalysis using Fe-doped ZnO nanoparticles.* Scientific reports, 2017. **7**(1): p. 1-14.
12. Valenzuela, L., et al., *Antimicrobial surfaces with self-cleaning properties functionalized by photocatalytic ZnO electrosprayed coatings.* Journal of hazardous materials, 2019. **369**: p. 665-673.

13. Gadhi, T.A., et al., *Evaluation of the photodiscoloration efficiency of β-Bi2O3 films deposited on different substrates by pneumatic spray pyrolysis.* Thin Solid Films, 2017. **638**: p. 119-126.
14. Anku, W.W., S.O. Oppong, and P.P. Govender, *Bismuth-based nanoparticles as photocatalytic materials.* Bismuth: Advanced Applications and Defects Characterization, 2018: p. 25.
15. Reverberi, A.P., et al., *Bismuth oxide-related photocatalysts in green nanotechnology: A critical analysis.* Frontiers of Chemical Science and Engineering, 2018. **12**(4): p. 878-892.
16. Coronado-Castañeda, R., et al., *Photocatalytic degradation and toxicity reduction of isoniazid using β-Bi2O3 in real wastewater.* Catalysis Today, 2020. **341**: p. 82-89.
17. Gadhi, T.A., et al., *Efficient α/β-Bi2O3 composite for the sequential photodegradation of two-dyes mixture.* Ceramics International, 2016. **42**(11): p. 13065-13073.
18. Ratova, M., et al., *Highly efficient photocatalytic bismuth oxide coatings and their antimicrobial properties under visible light irradiation.* Applied Catalysis B: Environmental, 2018. **239**: p. 223-232.
19. Ballo, M.K., et al., *Bactericidal activity and mechanism of action of copper-sputtered flexible surfaces against multidrug-resistant pathogens.* Applied microbiology and biotechnology, 2016. **100**(13): p. 5945-5953.
20. Son, H., et al., *Inhibition of Staphylococcus aureus by antimicrobial biofilms formed by competitive exclusion microorganisms on stainless steel.* International Journal of Food Microbiology, 2016. **238**: p. 165-171.
21. Li, Y., et al., *Promoting LED light driven photocatalytic inactivation of bacteria by novel β-Bi2O3@ BiOBr core/shell photocatalyst.* Journal of Alloys and Compounds, 2020. **816**: p. 152665.
22. Hudzicki, J., *Kirby-Bauer disk diffusion susceptibility test protocol.* 2009.
23. Hou, J., et al., *In situ synthesis of α–β phase heterojunction on Bi2O3 nanowires with exceptional visible-light photocatalytic performance.* Applied Catalysis B: Environmental, 2013. **142–143**: p. 504-511.
24. Ivanov, S., et al., *Structural studies of α-Bi 2 O 3 by neutron powder diffraction.* Powder Diffraction, 2001. **16**(04): p. 227-230.
25. Salazar-Pérez, A., et al., *Structural evolution of Bi2O3 prepared by thermal oxidation of bismuth nano-particles.* Superficies y vacío, 2005. **18**(3): p. 4-8.
26. Gadhi, T.A., et al., *Insights on the role of β-Bi2O3/Bi5O7NO3 heterostructures synthesized by a scalable solid-state method for the sunlight-driven photocatalytic degradation of dyes.* Catalysis Today, 2019. **321**: p. 135-145.
27. Gong, S., et al., *Controlled synthesis of bismuth-containing compounds (α-, β-and δ-Bi 2 O 3, Bi 5 O 7 NO 3 and Bi 6 O 6 (OH) 2 (NO 3) 4· 2H 2 O) and their photocatalytic performance.* CrystEngComm, 2015. **17**(47): p. 9185-9192.
28. Li, J., Y. Yu, and L. Zhang, *Bismuth oxyhalide nanomaterials: layered structures meet photocatalysis.* Nanoscale, 2014. **6**(15): p. 8473-8488.
29. Jiang, J., G. Oberdörster, and P. Biswas, *Characterization of size, surface charge, and agglomeration state of nanoparticle dispersions for toxicological studies.* Journal of Nanoparticle Research, 2009. **11**(1): p. 77-89.
30. Hernández-Gordillo, A., et al., *Good practices for reporting the photocatalytic evaluation of a visible-light active semiconductor: Bi 2 O 3, a case study.* Catalysis Science & Technology, 2019. **9**(6): p. 1476-1496.
31. Hernández-Gordillo, A., et al., *Photodegradation of Indigo Carmine dye by CdS nanostructures under blue-light irradiation emitted by LEDs.* Catalysis Today, 2016. **266**: p. 27-35.
32. Gadhi, T.A., et al., *Single BiFeO3 and mixed BiFeO3/Fe2O3/Bi2Fe4O9 ferromagnetic photocatalysts for solar light driven water oxidation and dye pollutants degradation.* Journal of industrial and engineering chemistry, 2018. **63**: p. 437-448.

33. Chiadò, A., et al., *Opening study on the development of a new biosensor for metal toxicity based on Pseudomonas fluorescens pyoverdine.* Biosensors, 2013. **3**(4): p. 385-399.
34. Ghugal, S.G., S.S. Umare, and R. Sasikala, *Enhanced photocatalytic activity of TiO 2 assisted by Nb, N and S multidopants.* Materials Research Bulletin, 2015. **61**: p. 298-305.
35. Deng, F., et al., *Fabrication of Hierarchically Porous Reduced Graphene Oxide/SnIn4S8 Composites by a Low-Temperature Co-Precipitation Strategy and Their Excellent Visible-Light Photocatalytic Mineralization Performance.* Catalysts, 2016. **6**(8): p. 113.
36. Chauhan, M., et al., *Investigating the efficiency of α-Bismuth zinc oxide heterostructure composite/UV-LED in methylene blue dye removal and evaluation of its antimicrobial activity.* Environmental Research, 2020. **180**: p. 108857.
37. Memar, M.Y., et al., *Antimicrobial use of reactive oxygen therapy: current insights.* Infection and drug resistance, 2018. **11**: p. 567.
38. Dryden, M., *Reactive oxygen species: a novel antimicrobial.* International journal of antimicrobial agents, 2018. **51**(3): p. 299-303.
39. Yuan, Y.-G., Q.-L. Peng, and S. Gurunathan, *Effects of silver nanoparticles on multiple drug-resistant strains of Staphylococcus aureus and Pseudomonas aeruginosa from mastitis-infected goats: an alternative approach for antimicrobial therapy.* International journal of molecular sciences, 2017. **18**(3): p. 569.
40. Paccotti, N., et al., *Label-free SERS discrimination and in situ analysis of life cycle in Escherichia coli and Staphylococcus epidermidis.* Biosensors, 2018. **8**(4): p. 131.
41. Ribeiro, M.A., et al., *Photocatalytic and photoelectrochemical inactivation of Escherichia coli and Staphylococcus aureus.* Water Science and Technology: Water Supply, 2015. **15**(1): p. 107-113.
42. Mandell, G., *Catalase, superoxide dismutase, and virulence of Staphylococcus aureus. In vitro and in vivo studies with emphasis on staphylococcal--leukocyte interaction.* The Journal of clinical investigation, 1975. **55**(3): p. 561-566.
43. Ferreira, A.A., et al., *Detection of exopolysaccharide production and biofilm-related genes in Staphylococcus spp. isolated from a poultry processing plant.* Food Science and Technology, 2014. **34**(4): p. 710-716.